Annual continuous fields of woody vegetation structure in the Lower Mekong region from 2000-2017 Landsat time-series

P. Potapov[a,*], A. Tyukavina[a], S. Turubanova[a], Y. Talero[a], A. Hernandez-Serna[a], M.C. Hansen[a], D. Saah[b], K. Tenneson[c], A. Poortinga[c,d], A. Aekakkararungroj[d,e], F. Chishtie[d,e], P. Towashiraporn[d,e], B. Bhandari[d,e], K.S. Aung[d,e], Q.H. Nguyen[d,e]

[a] University of Maryland, United States of America
[b] University of San Francisco, United States of America
[c] Spatial Informatics Group, United States of America
[d] SERVIR-Mekong, Thailand
[e] Asian Disaster Preparedness Center, Thailand

ARTICLE INFO

ABSTRACT

Spatially and temporally consistent vegetation structure time-series have great potential to improve the capacity for national land cover monitoring, to reduce latency and cost of international reporting, and to harmonize regional land cover characterizations. Here we present a semi-automatic, operational algorithm for mapping and monitoring of woody vegetation canopy cover and height at a regional scale using freely available Landsat time-series data. The presented algorithm employs automatic data processing and mapping using a set of lidar-based vegetation structure prediction models. Changes in vegetation cover are detected separately and integrated into the structure time-series. Sample-based validation and inter-comparison with existing datasets demonstrates the spatial and temporal consistency of our regional data time-series. The dataset reliably reflects changes in tree cover (tree cover loss user's accuracy of 0.84 and producer's accuracy of 0.75) and can serve as a tool to map annual forest extent (user's accuracy of 0.98 and producer's accuracy of 0.81 for 10% canopy cover threshold to define the forest class). The tree height estimates are consistent with a GLAS-based global map (mean average error of 3.7 m, the correlation coefficient of 0.92 and the R^2 of 0.85). The algorithm was prototyped within the Lower Mekong region where it revealed an intensive woody vegetation dynamic. Of the year 2000 forest area (defined using canopy cover threshold of 10% and tree height threshold of 5 m), 9.4% was deforested by the year 2017, and 16.6% was affected by stand-replacement disturbance followed by reforestation. The average annual area of stand-level forest disturbance within the region was 2.34 Mha, and increased by 34% from 2001 (1.85 Mha) to 2017 (2.48 Mha). Total forest area decreased by 6.2% within the region, and 11.1% of year 2000 primary forest area was lost by 2017. At the national level, Cambodia demonstrated the highest rate of deforestation, with a net forest area loss of 22.5%. We estimated that 21.3% of 2017 forest cover had an age of 17 years or less, illustrating the intensive forest land uses within the region. The time-series product is suitable for mapping annual land cover and inter-annual land cover change using customized class definitions. The regionally-consistent data are publicly available for download (https://glad.umd.edu/), and online analysis (https://rlcms-servir.adpc.net/en/forest-monitor/), and serve as an input to the SERVIR-Mekong Regional Land Cover Monitoring System.

1. Introduction

Approaches and algorithms for satellite data processing and time-series characterization have been developed since the mid-1980s through advancing computing capabilities and data analysis tools (Justice et al., 1985; Colwell, 1993; Brown et al., 1993). Due to computation and data access constraints, these methods were first applied at low spatial resolution using data from meteorological satellites (DeFries and Townshend, 1994; Loveland and Belward, 1997; DeFries et al., 1998). In the early 2000s, the development of satellite earth

---

observation technologies, digital data processing algorithms, and data distribution policies enabled the operational monitoring of global land cover at locally relevant spatial resolutions. The progress in using free-of-charge, consistently processed Moderate Resolution Imaging Spectroradiometer (MODIS) data (Friedl et al., 2002; Hansen et al., 2003, 2010) that enabled land cover mapping at 250 m spatial resolution was expanded to the Landsat data archive upon its opening for public access in 2008 (Woodcock et al., 2008). Landsat data, while lacking the high frequency of observations compared to MODIS, provided a medium (30 m) spatial resolution suitable for most land cover monitoring applications. Given its four-decade long history, many large-scale land cover change studies were made possible (Wulder et al., 2012).

Landsat data were found especially useful for forest monitoring due to its spatial resolution, spectral bandwidths, and observation frequency. Periodic monitoring of such key environmental parameters as tree canopy cover, composition, and disturbance are feasible with Landsat data (Iverson et al., 1989; Westman et al., 1989; Cohen and Goward, 2004). Early approaches based on discrete land cover classification and bi-temporal change detection (Tucker et al., 1984; Skole and Tucker, 1993) evolved toward modeling of continuous vegetation structure (DeFries et al., 1998; Hansen et al., 2002a, 2002b, Cohen et al., 2003) and function (Running et al., 2004). Change detection advanced through the use of dense time-series analyses (Huang et al., 2010; Kennedy et al., 2010; Verbesselt et al., 2010; Hansen et al., 2013) and integration of directly detected changes with annual land cover information (Potapov et al., 2015; Wulder et al., 2018). Non-parametric machine learning algorithms allowed extrapolating continuous forest composition and structure parameters by relating field observations to Landsat spectral reflectance data (Reese et al., 2003; Tomppo et al., 2008). Lidar-based forest structure data offer the possibility of integration with Landsat data through the use of lidar-derived canopy and height information for model calibration (Hudak et al., 2002; Wulder et al., 2007; Hansen et al., 2016; Matasci et al., 2018). We consider the airborne lidar data preferable for model calibration due to the inconsistencies in tree height estimation and the coarse spatial resolution of the Geoscience Laser Altimeter System (GLAS) data (Hansen et al., 2016). However, publicly available airborne data are scarce and may not be readily available for a particular region of interest.

Time-series of continuous vegetation structure (like tree canopy cover and height) may be used to detect changes that persist in time (Huang et al., 2010; Matasci et al., 2018). However, such an approach may not be suitable for tropical regions where clear-sky observation frequency is low, land cover change rapid, and tree canopy recovery fast following disturbance. Mapping tree cover structure and composition requires land surface phenology information collected over a growing season (or the entire year in the tropics, Hansen et al., 2016) while disturbance detection relies on reflectance change over shorter time intervals. Souza et al. (2005) showed that a single observation is often the only information available to detect ephemeral disturbance in tropical environments. To date, prototype tree cover structure models (Simard et al., 2011; Matasci et al., 2018) have relied on static topography and location metrics in addition to spectral variables, which may limit the ability to detect frequent changes in tree canopy cover.

Timely forest monitoring is a required precondition to the successful implementation of national policies and international agreements toward the ultimate goal of balancing economic development and environmental sustainability. As part of the United Nations Framework Convention on Climate Change (UNFCCC) and Reducing Emissions from Deforestation and forest Degradation (REDD+) program, countries are required to provide periodic reports on the state of their forests and carbon emissions related to forest conversion. Publicly available satellite data, specifically Landsat, benefit national forest monitoring systems, especially in developing countries where field-based forest assessments are often not fully operational and funds for commercial remotely sensed data purchase limited. All Lower Mekong countries, including Cambodia, Laos, Myanmar, Thailand, and Vietnam, use remotely sensed data to support National Forest Resource Assessments (FRA) (FAO, 2016) and REDD+ Forest Reference Emission Levels (FREL) reporting (MARD, 2016; MOE, 2017; MONREC, 2018; DOF, 2018).

The capacity of national monitoring agencies to process and analyze remotely sensed data is gradually improving, in part through support by programs such as SilvaCarbon (an interagency technical cooperation program of the U.S. Government) and SERVIR (a partnership project between NASA and the U.S. Agency for International Development). However, a number of constraints persist including limitations in data processing and analysis capacity, low data transparency and method replicability, and inconsistency of national map products between countries and time intervals. Post-classification comparison is frequently used for forest monitoring within Lower Mekong countries (MARD, 2016; MOE, 2017; MONREC, 2018). Such an approach is difficult especially if maps are made using different source data and, in some cases, produced by different expert teams using different methods and definitions. Manual digitizing (Vietnam) and manual attribution of image segments (Laos, Cambodia) are more frequently applied than automatic classification tools. In most cases, forest area and change are directly estimated from maps without implementing a statistical sampling approach as recommended by the "good practice" guidance for land cover and land cover change area reporting (GFOI, 2016; IPCC, 2006; Olofsson et al., 2014). Availability of regional spatially and temporally consistent data products, specifically forest extent, structure, and change, may be beneficial in such circumstances. The global tree canopy cover extent and change data (Hansen et al., 2013) distributed by Global Forest Watch (GFW, https://www.globalforestwatch.org/), an initiative of the World Resources Institute, are employed by many developing countries to support national forest change reporting. Regional time-series of continuous vegetation structure maps provide an alternative solution for national land cover mapping. Unlike discrete classification and change detection maps, such products may be integrated to create a national forest map using a specific set of forest class definitions. The Regional Land Cover Monitoring System (RLCMS) being developed by SERVIR-Mekong (2015) is using this approach to deliver spatially and temporally consistent time-series data for national land cover mapping and monitoring applications. The use of regionally consistent woody vegetation composition and structure time-series supports national forest monitoring programs and promotes regional consistency of reports while preserving national ownership of the derived maps and estimates.

The presented research has two primary objectives. The first objective is to develop a methodology for a comprehensive regional woody vegetation structure monitoring system that provides exhaustive data for national applications. Data users (including governmental, environmental, and academic organizations) are able to apply specific thresholds and definitions and to derive specific policy-related forest extent and type maps without the need to perform costly and complicated re-analysis of remotely sensed imagery. Our methodology is based on the automated Landsat data processing (Hansen et al., 2008; Potapov et al., 2012) and continuous tree canopy cover (Hansen et al., 2003) and height (Hansen et al., 2016) mapping methods. The methodology was prototyped in the Lower Mekong region for the 2000–2017 time interval, and the output products were validated using available reference data. Our second objective is to supply annual vegetation structure data to the SERVIR-Mekong RLCMS. The regionally-consistent dataset is publicly available for download (https://glad.umd.edu/) and online analysis (https://rlcms-servir.adpc.net/en/forest-monitor/). The SERVIR-Mekong and GFW teams are committed to its operational annual updates. The presented data have a potential to reduce effort and latency for national annual forest monitoring and to improve the quality and regional consistency of forest area and change reporting.

2. Data and methods

The study area, hereafter referred to as the Lower Mekong region, includes five countries: Cambodia, Laos, Myanmar, Thailand, and Vietnam. The analysis was done within country boundaries from the Database of Global Administrative Areas (GADM, www.gadm.org) and a 5-km buffer along the coastline to account for small islands that may be missing in the GADM data.

The Landsat Analysis Ready Data (ARD) produced by the Global Land Analysis and Discovery (GLAD) automated image processing system served as a data source for annual vegetation structure mapping. The essence of the GLAD ARD approach is to convert individual Landsat images into a time-series of 16-day normalized surface reflectance composites with minimal atmospheric contamination. The Landsat data processing algorithms were prototyped by Hansen et al. (2008) and Potapov et al. (2012). Since the development of the 2000–2012 forest loss product (Hansen et al., 2013), we improved the GLAD Landsat processing algorithm by re-calibrating quality assessment models, improving the reflectance normalization algorithm, and introducing a 16-day compositing method (consistent with MODIS Level 3 products, Huete et al., 1999) to store processed ARD. The Landsat ARD time-series data are subsequently used to generate different sets of multi-temporal metrics that serve as inputs to regional woody vegetation structure mapping and change detection (Fig. 1).

2.1. Landsat analysis-ready data time-series

In this study, we used the entire archive of Landsat TM, ETM +, and OLI/TIRS data collected from the year 1997 to 2017 within the Lower Mekong region. The source Landsat Collection 1 (Tier 1) data are available from the United States Geological Survey National Center for Earth Resources Observation and Science (USGS EROS) archive (https://earthexplorer.usgs.gov/). Overall, we processed 55,972 individual images from the archive. The Landsat ARD processing included four steps: (1) conversion to radiometric quantity, (2) observation quality assessment, (3) reflectance normalization, and (4) temporal integration into 16-day composites.

At the first step, all data were converted to top-of-atmosphere reflectance (Chander et al., 2009) for six reflective bands (excluding panchromatic band and OLI band 1) and brightness temperature for the emissive band. Spectral reflectance (value range from zero to one) was rescaled to the range from 1 to 40,000; temperature was recorded as degrees C multiplied by 100 to preserve measurement precision.

During the second step, we determined per-pixel observation quality, i.e. the probability of an image pixel to be collected during clear sky conditions. The GLAD quality assessment model represents a set of regionally adapted bagged decision trees (seven trees for each model) to map probability of a pixel to represent cloud, cloud shadow, heavy haze, and, for clear-sky observations, land or water. The decision tree models were similar to the one developed for Landsat processing in mapping global forest cover loss (Hansen et al., 2013), but were improved for the Lower Mekong region by adding training data from images where omission or commission errors were observed. The Landsat Collection 1 data include observation quality layers based on the globally consistent CFMask cloud and cloud shadow detection algorithm (Foga et al., 2017). Since our primary goal was to reduce the presence of clouds and shadows in the time-series data, we merged both CFMask product (high-probability clouds and shadows) with the GLAD algorithm output. This way, cloud, shadow, haze, water, and land masks were created for each Landsat image.

The third step consisted of reflectance and brightness temperature normalization to reduce the effects of atmospheric scattering and surface anisotropy (Potapov et al., 2012). The purpose of relative normalization is to facilitate the extrapolation of classification models in space and time by ensuring spectral similarity within land cover types. Relative normalization is not computationally expensive and does not require synchronously collected or historical data on atmospheric properties and land cover specific anisotropy, hence our preference of relative normalization over process-based atmospheric correction (Masek et al., 2006). The normalization target data were collected from the MODIS 44C surface reflectance product (Carroll et al., 2010). We used MODIS bands with a similar wavelength to the Landsat bands. To ensure spatial consistency of the reflectance target dataset, we used only near-nadir clear-sky and low aerosol observations collected for all 16-day MODIS composites from the year 2000 to 2011. We calculated the normalization target composite value as the mean reflectance of all observations having normalized difference vegetation index (NDVI) values above the 75% percentile. The Landsat image normalization consisted of three steps: (1) selection of pseudo-invariant target pixels to derive the normalization model; (2) model parametrization; and (3) model application for the entire image area. We defined the pseudo-invariant target pixels as clear-sky land observations that represent the same land cover type and phenology stage in the target Landsat image and MODIS normalization composite. To check for land cover type and condition, we calculated the absolute difference between Landsat and MODIS spectral reflectance for red and shortwave infrared bands and selected pixels with differences below 0.1 reflectance value for both spectral bands. Next, we calculated the median bias between MODIS and Landsat reflectance of pseudo-invariant pixels for each reflective band for each 10 km interval of distance from the Landsat ground track. The set of median values was used to parameterize a per-band linear regression model that predicts the reflectance bias as a function of distance from the ground track (similarly to the approach described in Potapov et al., 2012). The model was then applied to all pixels within the image to estimate the bias and subtract it from the Landsat top-of-atmosphere reflectance for each spectral band. To normalize the brightness temperature band, we used a mean bias value calculated from all pseudo-invariant target pixels.

The final step of Landsat time-series processing was temporal aggregation of individual images into 16-day composites. The compositing interval and the range of dates for each composite were selected corresponding to the Landsat orbital cycle and the MODIS Level 3 data products (Huete et al., 1999). Temporal compositing was done per-pixel using all overlapping observations within the 16-day interval. From all available observations, we retained the one with the highest observation quality as the composite value. Each 16-day composite contains normalized surface reflectance value for six spectral bands, normalized brightness temperature value, and the quality assessment code that attributes clear-sky and cloud/shadow contaminated observations. The 16-day interval composites are stored in geographic coordinates with a pixel size of 0.00025 degree.

The 16-day annual clear-sky data availability (Fig. 2, A) reflects the number of processed images per year. Data availability was low for the years 2001 and 2002, when a large fraction of Landsat 5 images were discarded due to sensor malfunction, and 2012 when only the Landsat 7 satellite was operational. The Lower Mekong region is located in a seasonal monsoon climate, and clear-sky data availability reflects seasonal cloud cover within the region (Fig. 2, B). The data distribution plots reveal the inconsistency of annual clear-sky data availability and suggest that a multi-temporal data aggregation and transformation is required to create spatially and temporally consistent inputs for annual mapping models.

2.2. Multi-temporal metrics

Multi-temporal metrics are a standard method of time-series data transformation. They were widely used for forest extent and structure monitoring at continental and global scales (DeFries et al., 1995; Hansen et al., 2013, 2016). We implemented the metrics approach to create consistent inputs for our annual vegetation mapping and change detection models and to overcome the inconsistency of clear-sky data availability that is typical for a humid climate. Two independent sets of
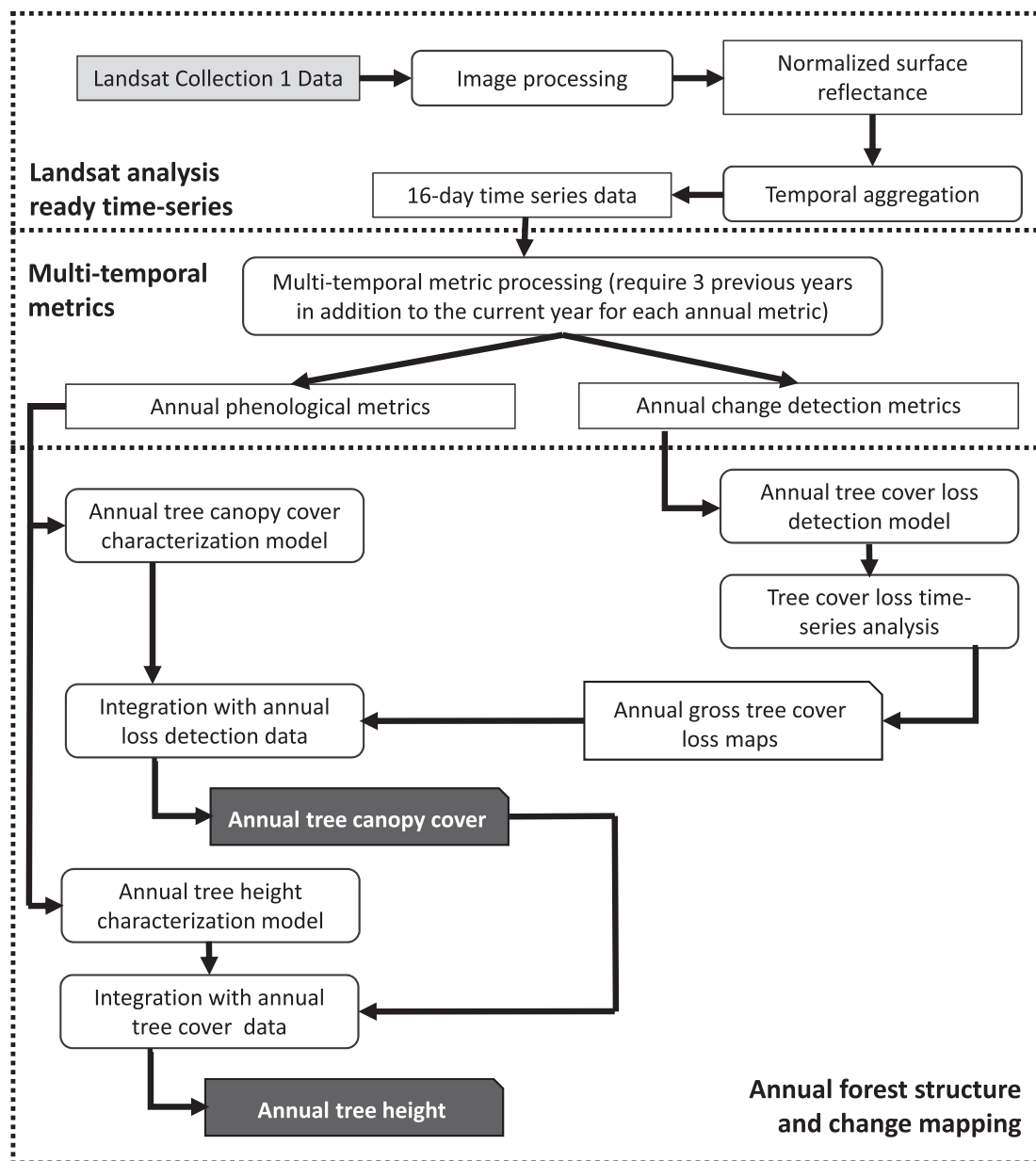
Fig. 1. Regional woody vegetation structure and change mapping workflow.

metrics were created from 16-day time-series data: annual phenological metrics and annual change detection metrics.

The annual phenological metrics were used as a source data for vegetation structure mapping. This metric set was derived from the 16-day reflectance data of the current year, while the data from the three previous years were used to fill gaps longer than two month in the observation time-series. Only observations with the best quality (lowest atmospheric contamination) were selected to calculate metric values. In addition to spectral reflectance and brightness temperature, we computed a spectral variability vegetation index (SVVI, Coulter et al., 2016) and a set of normalized band ratios using the following pairs of reflective bands: red/near-infrared (NIR), shortwave infrared (SWIR 1.6 μm)/NIR, blue/green, blue/NIR, green/red, green/NIR, and SWIR (1.6 μm)/SWIR (2.2 μm). A metric set represented a set of statistics calculated from the annual distribution of spectral reflectance and index values. First, all observations were ranked by each spectral band reflectance or index value individually. From obtained ranks, we extracted the highest/lowest, second to the highest/lowest values, values corresponding to the first, second, and third quartiles, and record them

as individual raster layers. In addition, we calculated averages for all observations between selected ranks and amplitudes between the highest and lowest values. Second, we distributed observation dates by the value of (i) NDVI, (ii) SVVI, and (iii) brightness temperature. From these distributions, we extracted observation dates corresponding to the highest/lowest, the second to highest/lowest and the first, second, and third quartiles of the ranked variable, recorded spectral reflectance of these observations, and calculated averages and amplitudes for observations between selected ranks. Metrics were independently calculated for each analysis year, 2000–2017.

The annual change detection metrics were designed to highlight inter-annual changes of spectral reflectance. We used all clear-sky 16-day observations from the current year, and observations for the same 16-day intervals from the preceding three years as a historical baseline for change detection. For each observation, in addition to normalized reflectance, we calculated normalized ratios from the following pairs of bands: red/NIR, SWIR (1.6 μm)/NIR, and SWIR (1.6 μm)/SWIR (2.2 μm). Similarly to the phenological metrics algorithm, we ranked spectral reflectance and indices values separately for the current and
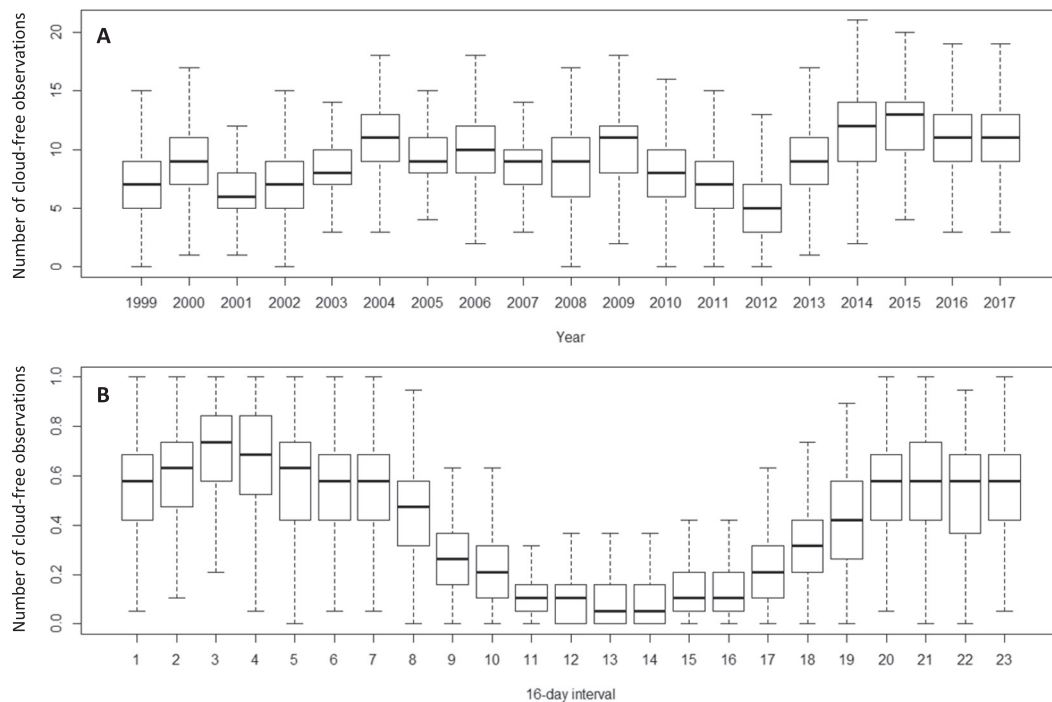
Fig. 2. Landsat clear-sky data availability for 3000 sample pixels selected for validation exercise (Section 2.5). A. An average annual clear-sky data availability (number of 16-day intervals with cloud- and shadow-free data). B. An average within-year clear-sky data availability for each 16-day interval.

preceding years, and extracted selected ranks and averages. We also ranked time-series observation dates by the corresponding NDVI and brightness temperature values and recorded spectral band values for selected ranks. To highlight changes in seasonal reflectance, we computed differences in spectral reflectance and indices values between the current and preceding year observations for the same 16-day interval, and extracted selected ranks (highest, second highest, lowest, second lowest) from the distribution of difference values.

In addition to multi-temporal spectral metrics, we used topography metrics (elevation and slope) derived from the void-filled seamless Shuttle Radar Topography Mission (SRTM) digital elevation data (http://srtm.csi.cgiar.org). The topography metrics served as inputs for both vegetation structure and change detection models.

2.3. Woody vegetation structure and change mapping

The objective of the presented method is to characterize time-series of tree canopy structure, specifically, tree canopy cover (proportion of land area covered by tree canopies) and tree height (the top height of tree crowns). Trees were defined as woody vegetation of 5 m or taller in height. We did not discriminate between natural tree cover and tree plantation and agroforestry, hence we used the term "woody vegetation". The term "forest" is used hereafter as a synonym of "woody vegetation" and does not refer to a land use category.

The airborne lidar-based canopy height model (CHM) served as calibration data for both tree canopy cover and tree canopy height regional products. The calibration data, however, were not available for the Lower Mekong region. To overcome this limitation, we modeled regional calibration data using lidar-based tree canopy cover and height models derived for other tropical forests. The source lidar data were collected by the G-LiHT instrument (Cook et al., 2013) over the United States and Mexico in 2013 and by ALTM 3100 lidar scanner over the Democratic Republic of the Congo (DRC) in 2014–2015 (Xu et al., 2017). The per-pixel CHM values were modeled from these observations at 1 m (the United States and Mexico) and 2 m (the DRC) resolution. The calibration data represent transects distributed to maximize the representation of different forest types. We aggregated the

high spatial resolution CHM maps into the 0.00025 × 0.00025 degree Landsat dataset resolution. For each Landsat pixel located within the lidar transect, we calculated canopy height (90% percentile height per pixel) and tree canopy cover (percent of pixel area with canopy height equal to or above 5 m). Additional calibration data (pixels with zero canopy cover and height) were manually collected over water (where lidar does not record returns) and treeless areas (especially, wet grasslands and irrigated croplands) that were found to have commission errors during model testing. Bagged regression tree ensembles (Breiman, 1996; Breiman et al., 1984) were used to relate the lidar-based tree canopy cover and height data as dependent variables and annual phenological metrics for the 2014–2016 years as independent variables in Mexico and the DRC, independently.

The Mexico and the DRC tree canopy cover and height mapping models were applied within the Lower Mekong region using the year 2016 metrics. We aggregated the outputs of Mexico and the DRC models taking the maximum predicted value per pixel, and used a random subset from the resulting dataset as a regional training data for the year 2016. We manually collected additional training sites to improve characterization of wetlands, including mangroves (Giri et al., 2011). The final bagged regression tree ensembles (25 trees for each model) were applied annually to the Lower Mekong region to produce tree cover height and cover per-pixel estimates.

The annual tree cover loss detection model was calibrated using manually collected training data. To create the training data set, we performed supervised classification to detect tree cover loss within 2013–2016 interval. The year with the highest drop of the NDVI was assigned as the year of change event within the change class mask (Hansen et al., 2013). We collected a random subset of training data from the 2013–2016 tree cover loss product and related it to the annual change detection metrics in order to derive a model applicable to all years. Mapping forest gain at the annual interval is challenging due to the gradual nature of tree growth. To map gain, we used the time series of vegetation structure metrics (e.g., tree cover and height increase) as the measure of tree growth.

After the annual tree canopy cover, height, and loss maps were completed, we implemented the stepwise integration of these products
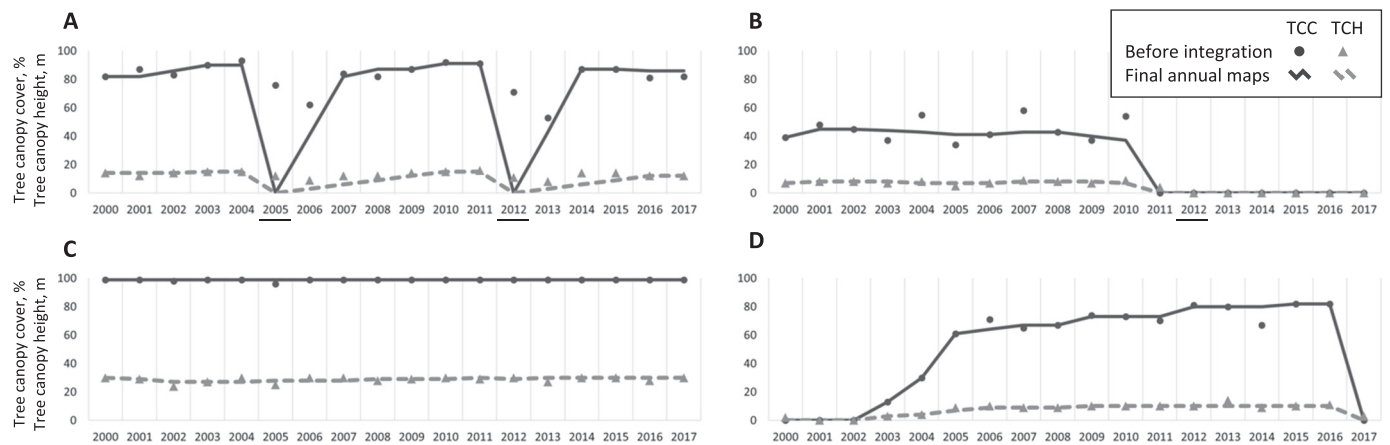
Fig. 3. Examples of annual tree canopy cover and height per-pixel estimates before and after integration with change detection time-series. Tree canopy cover (TCC) shown in percent and tree canopy height (TCH) in meters on the same scale. Years when tree cover loss was detected are underlined. A - Shifting cultivation land use. Bolikhamsai province, Laos. B - Primary lowland forest cleared for agriculture. Kampong Speu province, Cambodia. C - Primary forest. Ratchaburi province, Thailand. D - Rubber plantation established on a former agricultural land and cleared in the year 2017. Binh Duong province, Vietnam.

into a consistent time-series (Fig. 3). Our objectives were (i) to integrate tree cover loss data into annual woody vegetation structure time-series; (ii) to reduce high-frequency inter-annual noise in vegetation structure model outputs; and (iii) to improve the agreement between tree cover and height model outputs. For a year when a forest loss event was detected, the canopy cover and height was set to zero. Spikes in tree canopy cover and height were removed using a 3-year median. In case of high-frequency noise (the tree canopy cover or height oscillates between years), we replaced model outputs with values estimated using linear regression.

2.4. Primary forest mapping

To assess natural forest loss, we mapped long-lived natural forest extent, hereafter referred as "primary forests", for the year 2000. The primary forest definition and mapping was based on the approach developed by Turubanova et al. (2018) for humid tropical forests and modified to include dry and seasonal forest types. Only areas with tree canopy cover of 25% and higher in the year 2000 were considered. In order to detect effects of pre-2000 disturbance, we used Landsat TM data from the period of 1988 to 1999. We manually collected training data for the primary forest class to calibrate a classification model that employed year 2000 phenological metrics and 1988–2000 reflectance trend metrics (slope and standard deviation of reflectance values related to the observation date). The output map was manually edited to remove mature tree plantations established before 1988 and older secondary forests, both identified by shape and pattern features.

2.5. Sample-based validation

The objectives for sample analysis were (i) to validate the year 2016 tree canopy cover and 2001–2017 tree cover loss maps, and (ii) to identify populations of stable and dynamic tree cover pixels for the temporal consistency analysis of the annual tree cover maps. A random sample of 3000 Landsat pixels was selected within the Lower Mekong region. The reference interpretation for each sample pixel was performed by an image analyst using the following source data: annual Landsat clear-sky mean surface reflectance image composites, temporal profiles of 16-day NDVI, NIR/SWIR normalized ratio, and SWIR (1.6 μm) normalized surface reflectance, and available high-resolution time-series data on Google Earth. The availability of at least one high-resolution image in Google Earth was critical for land cover type and tree cover interpretation and sample pixels not covered with such data were excluded. While most of the samples had high-resolution images

for the year 2016, a small proportion (2.3%) of samples were interpreted using images from other years, ranging from 2013 to 2017. The total number of sample pixels for which reference data were collected was 2964 (missing data accounted for 1.2% of all sample pixels).

For each sample pixel, we recorded information about land cover and land use type, tree cover, and tree cover change. Land cover and tree canopy cover were interpreted using the latest (before the end of the year 2017) available high-resolution image on Google Earth. Land cover classes distinguished in the process of visual sample interpretation included: woody vegetation (separated into natural mature forests, young secondary forests, fallows, and tree plantations), shrublands, treeless wetlands, agriculture areas, open water, bare rocks, developed areas (that include rural settlements, urban areas, and infrastructure objects), and recently cleared areas. Tree canopy cover within each sample pixel was calculated as a proportion of nine regularly spaced sample points that intersect tree crowns within a 30x30m Landsat pixel. Tree cover change events were interpreted primarily using Landsat time-series data, with the help of available high-resolution images. We identified instances of tree cover loss, gain, and rotation (which includes loss events followed by tree gain, as well as tree cover establishment and subsequent clearing). Partial change events that affected only a fraction of a sample pixel were recorded as a separate set of classes (partial loss, gain, and rotation).

2.6. Inter-comparison with GLAS-derived vegetation height map

The absence of publicly available airborne lidar data for the Lower Mekong region precluded direct validation of the tree canopy height maps. The data collected by GLAS instrument onboard the NASA Ice, Cloud, and land Elevation Satellite (ICESat) between 2003 and 2009 offered an alternative source of reference data. However, the GLAS data are affected by the atmosphere and topography, and even after filtering, the data have multiple errors in canopy height estimation (Hansen et al., 2016). Alternatively, we decided to use the global GLAS-calibrated tree canopy cover map of a 1-km resolution produced for the year 2005 (Simard et al., 2011) that we resampled to the 30-m resolution. To perform inter-comparison, we selected a random sample of 10,000 Landsat pixels from the year 2005 tree height map. From this sample, we excluded pixels that (i) had any water fraction, (ii) experienced tree cover change, or (iii) pixels for which, due to differences in product resolution, one of the maps showed zero tree height while the other estimated it above 5 m. The remaining 3411 sample pixels were used for inter-comparison.

3. Results

3.1. Accuracy and consistency of the annual woody vegetation structure and change maps

The primary objective of our methodology is to generate spatially and temporally consistent woody vegetation structure products that can serve as a foundation for regional and national forest monitoring. Therefore, it is critically important to evaluate the quality and consistency of these products to demonstrate their suitability for the task. Direct accuracy assessment for long (18 years) vegetation structure time-series is not feasible in the region due to the absence of quality reference data. However, the temporal consistency of annual maps can be evaluated using sample-based data. In the following section, we present the accuracy and consistency of the vegetation structure time-series quantified using best available reference data for each product component.

3.1.1. Annual tree canopy cover

The reference data quantify tree canopy cover for the year of the latest high-resolution image available from Google Earth (n = 2964). We compared the reference data to map data for the same year within major land cover types (Fig. 4). The comparison showed that the map data consistently underestimated tree canopy cover for all land cover types except treeless areas. The observed underestimation is primarily related to the differences in canopy cover measurement. While the mapping model was calibrated with lidar data that is sensitive to within-canopy gaps, the reference data were interpreted using visual observations of canopy extent, or crown cover, and small gaps within and often between tree canopies are not discernable. Tree cover within settlements and agriculture areas was consistently underestimated due to high landscape heterogeneity, while treeless land covers were mapped well. Despite these underestimations, the map proved sufficient in discriminating forested and non-forested areas.

To quantify tree canopy cover map accuracy, we converted both reference and mapped tree canopy cover data into "forest" and "non-forest" classes. For the reference data, we used the 10% tree canopy cover threshold to define forest class, and for the map data, we defined forest as sample pixels with tree canopy cover of 10% or higher and tree height of at least 5 m. The accuracy statistics shows the overall accuracy of 0.86 (SE 0.006), the forest class user's accuracy of 0.98 (SE 0.004) and the producer's accuracy of 0.81 (SE 0.009). Omission (false

negatives) and commission (false positives) errors were largely attributed to sample pixels within heterogeneous agriculture and agroforestry landscapes and within shrub/savanna ecotones. Tree cover within predominantly treeless agriculture landscapes usually exists in small clusters, the area of which is smaller or similar to the Landsat pixel size. Such clusters may not be reliably detected in Landsat-scale mapping, as was demonstrated by our earlier research in Bangladesh (Potapov et al., 2017).

3.1.2. Tree cover loss detection

The accuracy of the tree cover loss detection was quantified using the same sample of 2964 Landsat pixels. Overall, 493 sample pixels that were identified during reference image interpretation as loss or rotation experienced a complete clearing of tree cover during the 2001–2017 interval. We labeled those pixels as positive tree cover loss detection and the rest of the pixels (including those with partial loss) as stable. The overall accuracy of the tree cover loss detection model was 0.93 (SE 0.005), with the loss class user's accuracy of 0.84 (SE 0.02) and producer's accuracy of 0.75 (SE 0.02).

3.1.3. Tree cover dynamics

For a user of the vegetation structure time-series products, the inter-annual changes in tree canopy cover serve as an indicator of forest dynamics. Using the reference tree cover dynamics types, we can demonstrate the consistency of time-series data and its suitability for tree cover change quantification. Sample pixels where tree cover change was observed (n = 567) demonstrate high amplitude of tree canopy cover for the 2000–2017 interval, with the median amplitude above 50% cover (Fig. 5, A). When loss and gain events were considered separately, the amplitude of tree cover loss and gain was consistent for unidirectional changes (Fig. 5, B and C). Sample pixels that were interpreted as tree cover loss (n = 130) exhibited high tree cover reduction (median tree cover loss of 54%) and low tree cover gain (median gain 16%). Tree cover gain sample pixels (n = 74) had a median tree cover loss of 5% and gain of 64%. Sample pixels interpreted as tree cover rotation (n = 363) exhibited both high tree cover loss (median 80%) and gain (median 70%). Sample pixels with partial change (where change event affected a portion of the pixel, n = 160) had higher tree cover amplitude compared to stable sample pixels. Sample pixels where reference data showed no tree cover change (n = 2223) had a low amplitude of tree cover (mean tree cover amplitude of 7.6% with the standard deviation of 12.2%). While sample pixels representing stable
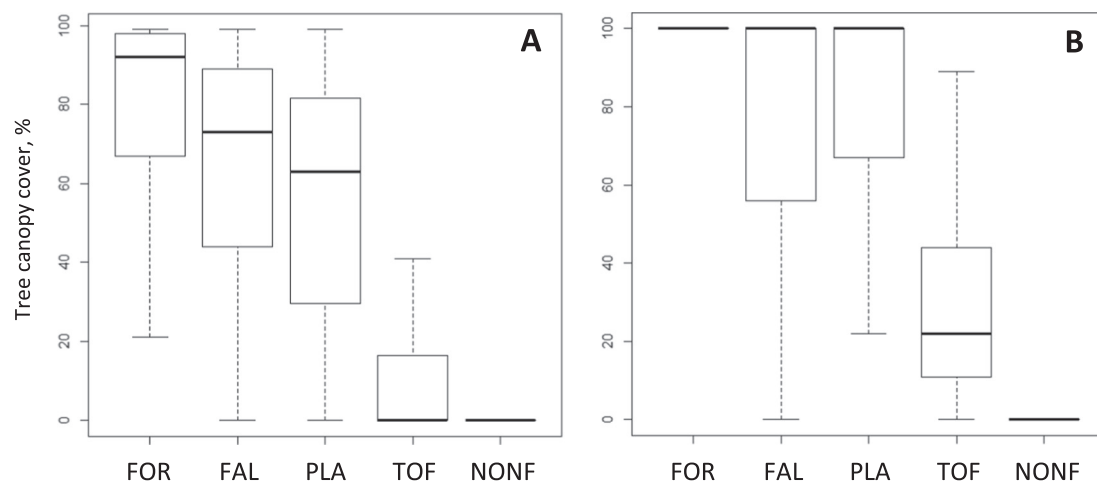

Fig. 4. Tree canopy cover for the year when a high-resolution image was available as a reference. A – mapped tree canopy cover, B – interpreted tree canopy cover. Land cover categories: FOR – forests; FAL – fallows, part of the shifting cultivation land use; PLA – tree plantations (including palms); TOF – land cover and land use categories with trees outside forests, including settlements, natural pastures, and savannas; NONF – treeless land cover and land use, including agriculture areas, water, rocks, and wetlands. The NONF class also includes all fresh clearing areas within plantation and shifting cultivation land uses that have no tree cover in both reference and map data.
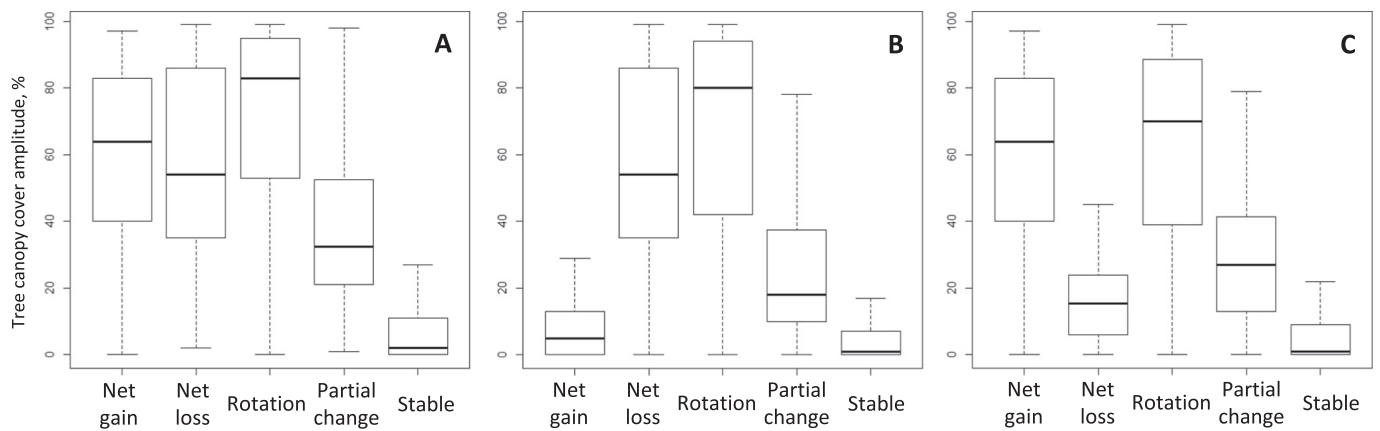
Fig. 5. Tree canopy cover amplitude as indication of forest dynamics. Inter-annual statistics include tree canopy cover amplitude (A), maximal tree canopy cover loss (B) and gain (C) within the time-series. The tree cover dynamics was attributed by experts using time-series of Landsat data and high resolution images available in Google Earth. The unidirectional changes were attributed as "Net gain" and "Net loss"; sample pixels that experienced both loss and gain events were included into the "Rotation" type; any type of partial change event was attributed as "Partial change"; and all other sample pixels were assigned to the "Stable" type.

land cover were clearly separable from loss and gain events, remaining inter-annual variation of mapped canopy cover values may result in change detection commission errors. Considering measured tree cover amplitude in "stable" sample pixels, we suggest to ignore pixels with less than 20% tree cover change when mapping high confidence forest loss or gain areas.

3.1.4. Tree canopy height

An inter-comparison of our tree canopy height map for the year 2005 with the global GLAS-derived vegetation canopy height (Simard et al., 2011) for sample pixels with stable land cover demonstrated strong agreement between these products. The mean average error (MAE) is 3.7 m, the correlation coefficient is 0.92 and the R^2 of linear regression of Simard et al. (2011) estimates vs. our estimates is 0.85. The mean error (ME) is 2.4 m and demonstrates some underestimation of our tree height map compared to the GLAS-based product (Fig. 6).

3.2. Forest dynamics in the Lower Mekong region

To illustrate trends in regional and national tree cover, we defined "forest" using the minimum inclusion threshold of 10% tree canopy cover and 5 m tree height. All area estimates hereafter are based on the map data unless specified otherwise. Of the total forest class area of the

Fig. 6. GLAS-modeled (Simard et al., 2011) vs. Landsat-derived (this research) estimates of the year 2005 tree canopy height for selected sample pixels ($n = 3411$). The gray level represents sample density.

year 2000 (119.6 million hectares, Mha), 9.4% was cleared by the year 2017, and 16.6% was affected by stand-replacement disturbance from the year 2001 to 2017. The area of the forest class in 2017 was 112.2 Mha. Of this area, 45.5% consist of stable primary forests, 17.2% experienced stand-level disturbance from the year 2001 to 2017, 3.8% of the year 2017 forests were established within the year 2000 non-forest area. The remaining 33.5% represented by secondary forests and plantations did not experience stand-level disturbance during the study period. The sample-based estimate of forest area (defined using the 10% canopy cover threshold) for the circa year 2016 was 133.5 Mha (95% confidence interval of $+/-$ 3.4 Mha).

By 2017, the region lost 11.1% of its year 2000 primary forest area. The rates of primary forest reduction were different among the countries. While Thailand lost only 4.2% of its primary forests, Cambodia lost almost 29%.

The regional forest dynamics analysis was performed for the years 2001–2015, allowing us to observe a two-year trend of forest recovery after disturbance event (Fig. 7). A "forest loss" label was assigned only to those areas that were classified as forests in 2000 and, after forest clearing between 2001 and 2015, did not restore tree cover by the year 2017. The new forest areas that were established after the year 2000 and did not experience disturbance events from 2001 to 2015 we considered "forest gain". All other areas that experienced stand-level disturbance were considered "forest rotation". Our analysis for the year 2015 shows that 32.1% of the maximum forest class area (all areas that were classified as forest for at least part of the 2000–2015 interval) experienced clearing and/or regeneration events. Only 27.1% of the Lower Mekong region total land area was covered by primary forests that did not experience changes during 2000–2015 interval. Among the countries, the largest share of dynamic forests was found in Cambodia and Vietnam, 39.3% and 38.5% of the maximum forest class area, respectively. Forest dynamics were dominated by tree cover rotation in all countries except Cambodia, where deforestation was the dominant forest dynamics trajectory.

The average annual area of forest clearing within the region is 2.34 Mha. The annual disturbance area increased from 2001 (1.85 Mha) to 2017 (2.48 Mha) by 34% (Fig. 8). A "spike" of forest clearing in 2013 corresponds to extensive deforestation in Cambodia.

Inconsistent national forest definitions and land use management categories impede the comparison between our biophysically-derived forest area and the official country forest area reports. We compared our forest area estimates with the national forest area submitted by the countries to the most recent FAO FRA report (FAO, 2016). The FAO data are provided for the years 2000, 2005, 2010, and 2015. For the purpose of this inter-comparison, we have aggregated reported "forest"
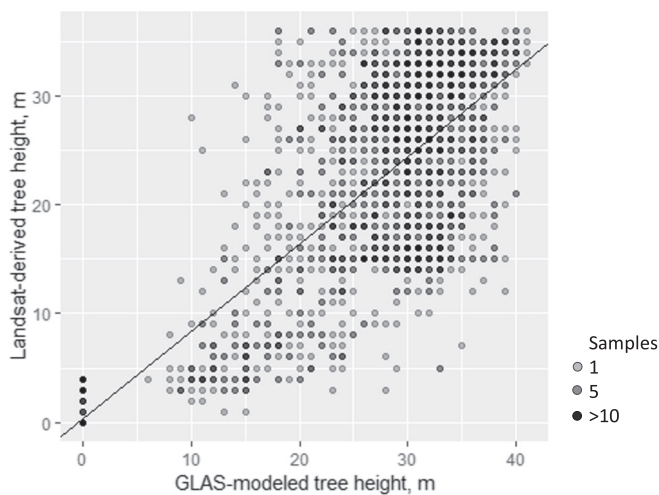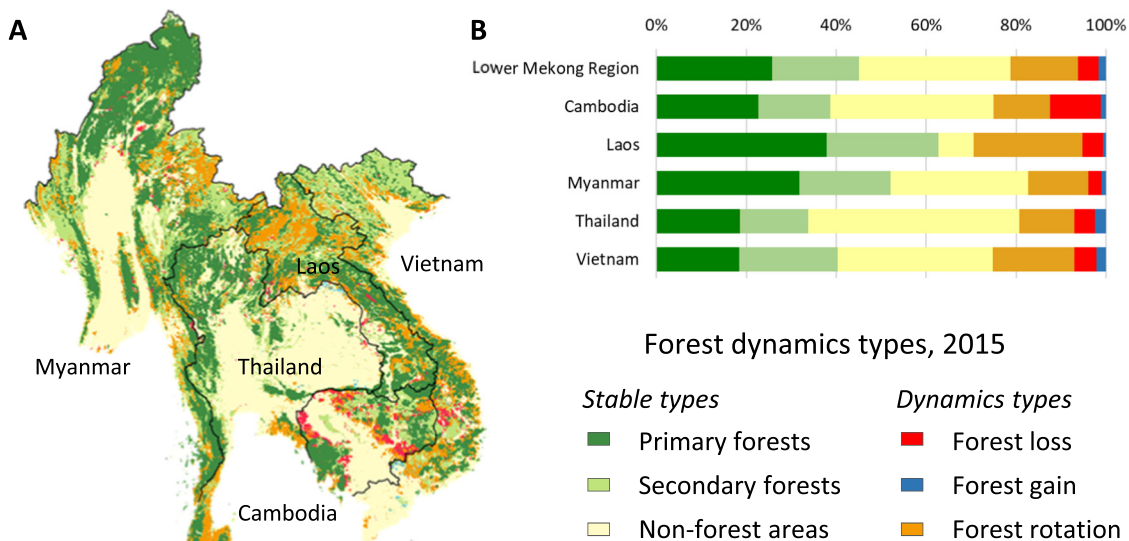
Fig. 7. Forest dynamics within the Lower Mekong region, 2000–2015. A – The dominant forest dynamics type for each 3×3 km grid cell. B – Proportion of forest dynamics types from the total land area.
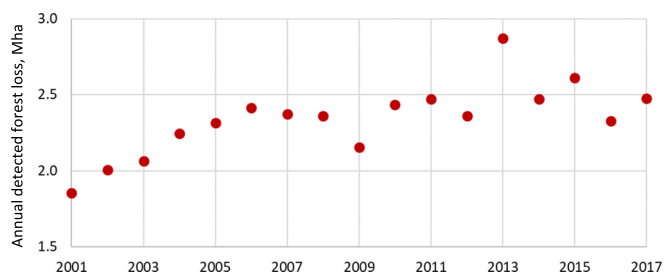

Fig. 8. Annual gross forest loss, million hectares (Mha).

and "other wooded land" area for each country. Our annual vegetation structure maps were converted into the "forest" class using 10% and 30% canopy cover and 5 m tree height thresholds. Both FAO data and our time-series maps indicate the decrease of forest area within the region (Fig. 9). We estimated that the year 2000 forest area decreased by 6.2% using a tree canopy cover threshold of 10% and by 3.9% for a 30% threshold. The difference may be explained by the disproportionally high deforestation within dry deciduous open-canopy forests in Cambodia and Vietnam. Of all countries, only in Cambodia do our Landsat-based results and the national FRA report show similar forest areas and inter-annual trend. In Laos and Myanmar, our estimates are similar to the official reports at the beginning of the interval (in Laos, 2% difference in 2000) or the end of the interval (in Myanmar, 2% difference in 2015). However, for the rest of the interval, our estimates diverge from the national reported forest area. In Laos, the Landsat-based forest area depicted a 7.5% net loss by the year 2017, while the FRA reports a 6% gain in forest area by the year 2015. In Thailand and Vietnam, the Landsat-based forest area estimates are much higher compared to official reports (by 43% and 31%, respectively), which may be explained by the fact that these countries employ a land-use based forest definition that excludes orchards, non-timber plantations, and agroforestry. The Landsat-based forest area in Vietnam declined by 6% by the year 2017, while the FRA-reported forest area increased.

Forest disturbance dynamics were used to estimate the age of forest stands within the region (Fig. 10). We define forest age as the number of years since a particular area reached a set of forest class thresholds (tree canopy cover of 10% or higher and tree height of 5 m or taller). Overall,

21% of the year 2017 forests had an age of 17 years or less. Vietnam and Laos exhibit the highest share of forests younger than 18 years, 26.5% and 24.2% of the year 2017 forest extent, respectively. Young forests mostly consist of fallows and tree plantations. Fallow age is one of the most important variables required for carbon balance modeling within shifting cultivation landscapes (DOF, 2018). Our forest dynamics products provide key variables for national and regional carbon balance modeling.

4. Discussion

4.1. Advantages and applications of vegetation structure time-series

The use of high spatial resolution satellite data, such as Landsat, for national and regional analysis of ecosystem functions and dynamics is growing. However, the image mass-processing, long time-series analysis, and large-area consistent data characterization are still challenging for most data users. Off-the-shelf, spatially and temporally consistent products that represent basic characteristics of land cover and change would allow users to implement satellite-based data for national and regional reporting and modeling without the need to apply all data processing steps (SERVIR-Mekong, 2015).

The best example of the hierarchical data processing chain and high-level product suite was demonstrated by the MODIS science team. The science team established a systematic data processing structure adopted by NASA for other earth observations datasets (Justice et al., 2002). We build our Landsat processing algorithm following the MODIS data processing principles. The source Level 1 data (geometrically corrected and radiometrically calibrated) is stepwise processed to Level 2 (normalized surface reflectance), and Level 3 (temporally aggregated 16-day observation time-series). Level 3 ARD is used as input data to generate annual multi-temporal metrics that represent land surface phenology and inter-annual changes of spectral reflectance. Our mapping models are based on these inputs, and model outputs (tree canopy cover, tree height, and tree cover loss) are integrated into a spatially and temporally consistent Level 4 product suite appropriate for national land cover and change monitoring applications.

While the consistency and accuracy of vegetation structure time-series are validated in the current study, users should be aware of errors inevitably present in wall-to-wall maps. For national reporting, the land
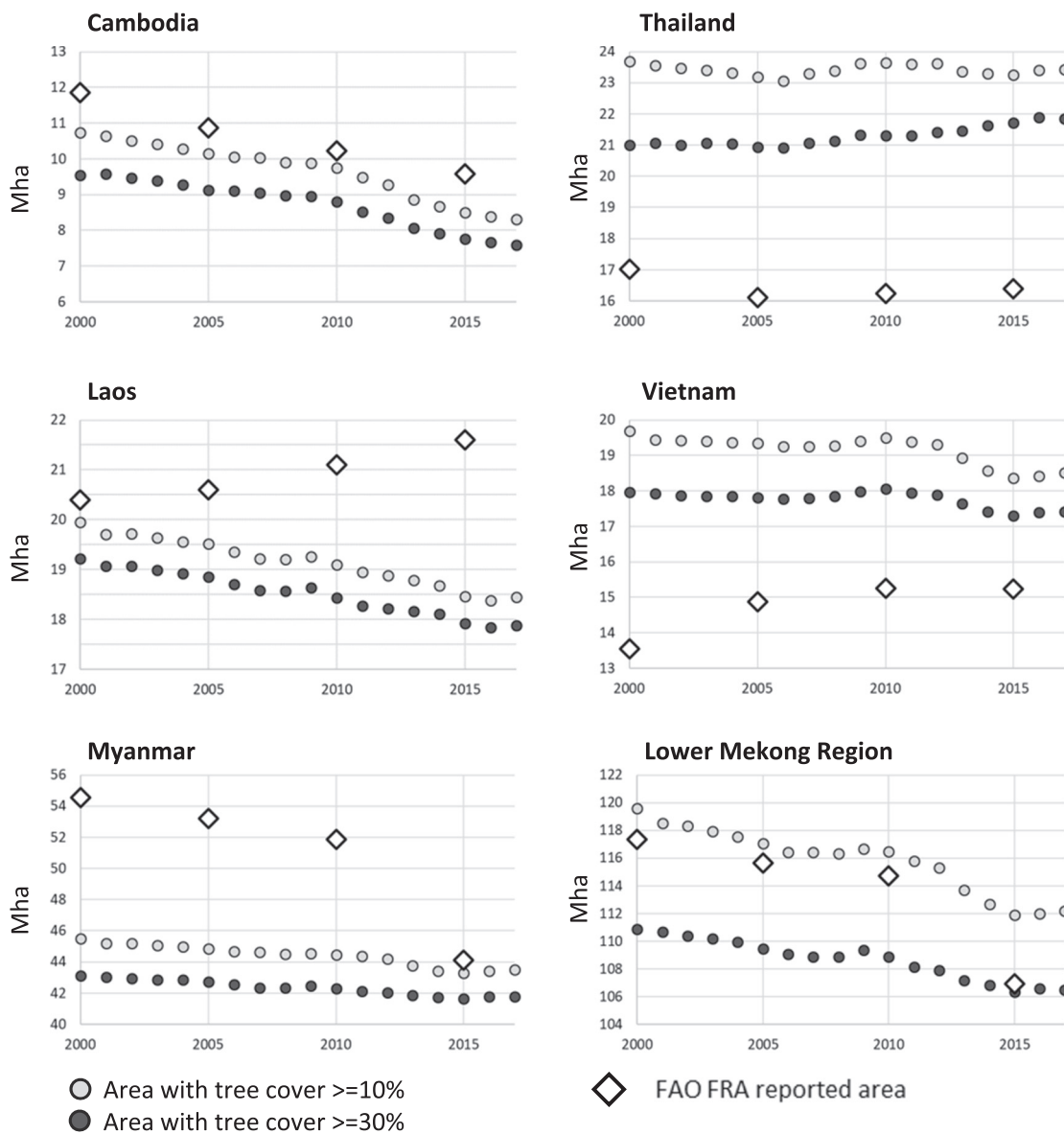
Cambodia

Thailand

Laos

Vietnam

Myanmar

Lower Mekong Region

○ Area with tree cover >=10%
● Area with tree cover >=30%
◇ FAO FRA reported area

Fig. 9. Annual forest class area from the current study, defined using tree canopy height threshold of 5 m or taller and tree canopy cover threshold of 10% and 30%, and the national forest and other wooded land area for the years 2000, 2005, 2010, and 2015 reported to the FAO FRA (FAO, 2016).

cover and land cover change area should be estimated from reference sample data, preferably collected using higher spatial resolution inputs (IPCC, 2006; Olofsson et al., 2014; Potapov et al., 2014, 2017). The wall-to-wall vegetation structure time-series serves as an important component for sample-based analyses, specifically for stratification which improves sampling efficiency (Stehman, 2014; Tyukavina et al., 2013), and as an auxiliary variable for regression estimator procedures, improving the precision of the area estimate (Pickering et al., 2019).

4.2. The value of land surface phenology data for vegetation structure mapping

The tree canopy cover and height models were both derived using the same set of annual Landsat spectral reflectance phenological metrics. The most important variables that were used by these models are similar. Both models primarily employ annual reflectance averages and amplitudes that characterized per-pixel land surface phenology. From the five most important metrics for the tree canopy cover model, two are based on NDVI (annual average and average between the minimum and median values within the year). The other three are annual average

red reflectance, interquartile average green reflectance, and the average value of the normalized ratio of blue and red reflectance between the median and the maximum annual values. For the tree canopy height model, the most important metrics include annual averages of NDVI and SWIR (1.6 μm) reflectance and the averages between the minimum and maximum, first and second quartiles and minimum and median values of green reflectance. Elevation and slope did not feature significantly in the models, together contributing 1.9% and 1.2% of total deviance reduction for the canopy height and cover models, respectively. These results suggest that static variables, like topography, may be less important for the models that predict annual vegetation structure in a highly dynamic landscape. Previously, Matasci et al. (2018) showed that elevation and latitude are the most important metrics to explain vegetation structure. We suppose that while such models may have high prediction power in static landscapes or for a single year, they may fail to correctly predict changes in vegetation structure between years. For models that predict vegetation structure in dynamic landscapes, spectral metrics that are collected from annual observation time-series of vegetation phenology have the highest predictive power.

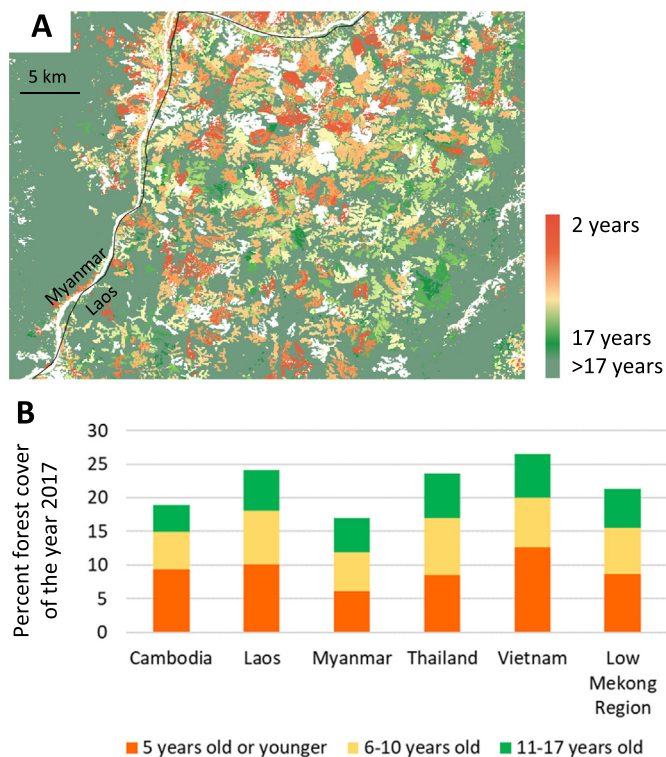The annual NDVI phenological metrics have the highest importance

Fig. 10. The age of forest stands in the year 2017. A – Forest age map subset in Luang Namatha province of Laos. B – Percent total year 2017 forest area by age class (forests older than 17 years are not shown).

in both canopy cover and height models, contributing 74% and 75% to the total deviance reduction, respectively. Thus, we may expect that forest seasonality will greatly affect predicted structure parameters, as shown by Hansen et al. (2016). The year 2016 tree canopy cover for the sample pixels interpreted as natural forests (n = 1320) showed high variability between forest types, defined using FAO climatic ecozones (FAO, 2001) (Fig. 11). While evergreen humid tropical and mountain forests exhibit high median canopy cover (above 90%) and low variability, the tree cover in moist and dry deciduous forests is lower and the variability of tree cover is higher. The reference data, collected using high-resolution images from Google Earth, reflected closed-canopy conditions for all forest types except dry forests which consist of open-canopy forests and savannas. As shown by Hansen et al. (2002a,
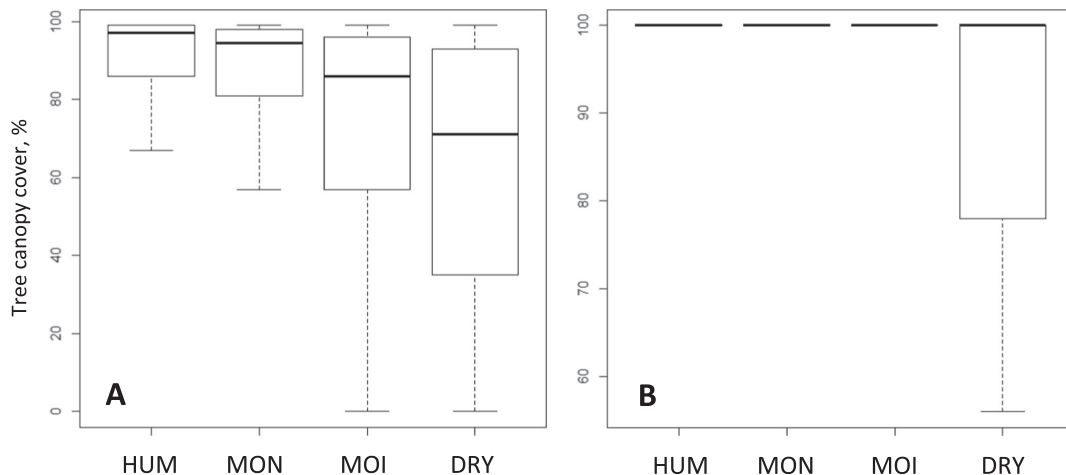
2002b), high spatial resolution satellite data do not enable the discrimination of small within-canopy and between-canopy gaps and surrounding tree canopies in dense forests. In our validation exercise, such areas were counted as closed canopy cover, which may inflate reference tree cover estimation.

The variation of clear-sky data availability is reflected in a subtle fluctuation of annual tree canopy cover and height predictions. When considering only stable, closed-canopy primary forests, we notice a year-to-year fluctuation of vegetation structure parameters, ranging $+/-$ 2% for tree canopy cover and $+/-$ 0.5% for tree canopy height around the 2000–2017 average (Fig. 12, A). We observe that these fluctuations are caused by dramatic changes in annual clear-sky data availability, ranging to $+/-$ 40% of the 2000–2017 average (Fig. 12, B). The lowest data availabilities were observed in 2001–2002 and 2012, resulting in a drop of annual average NDVI and anomalous vegetation structure estimation.

Extreme weather events that resulted in changes of annual vegetation phenology (droughts, floods) may affect annual vegetation structure prediction. Our data indicated a decrease of tree canopy cover and height within stable primary forests in the year 2016 (Fig. 12, A). The observed changes in the average tree cover and height were not distributed equally within primary forests but concentrated in the high mountain forests within the Annamite Range in Laos and Vietnam (Fig. 13, A-C). These forest areas were affected by a drought in 2015–2016 attributed to a strong El Niño event (Thirumalai et al., 2017). The drought, evident in Lower Mekong annual precipitation data (Fig. 13, D), affected high altitude forests with clear evidence of an average annual NDVI decrease (Fig. 13, E). The effect of the drought on tree mortality and forest structure is unknown and can only be confirmed via field research, which may be not possible in these remote areas. We observed a rapid recovery of NDVI in 2017. Thus, we may presume that the drought caused temporary defoliation, but did not dramatically alter forest structure.

4.3. The value of annual tree cover change detection data

In boreal and temperate regions, it takes a forest stand several years to reach 5-m height after stand-level disturbance. In such an environment, mapping annual tree cover (Huang et al., 2010; Matasci et al., 2018) is sufficient to capture forest dynamics. In tropical ecosystems, the tree cover and height recovery is much faster, especially within tree plantations. Given the high frequency of disturbance and forest recovery, mapping change areas from annual tree cover and height time-series is challenging. A forest disturbance event that occurs within a year affects only a portion of the annual reflectance time-series. In this

Fig. 11. Tree canopy cover for sample pixels interpreted as "natural forests". A – mapped tree canopy cover, B – interpreted tree canopy cover. Sample pixels are attributed by the FAO ecozones into humid forests (HUM), mountain forests (MON), moist deciduous forests (MOI), and dry forests (DRY).
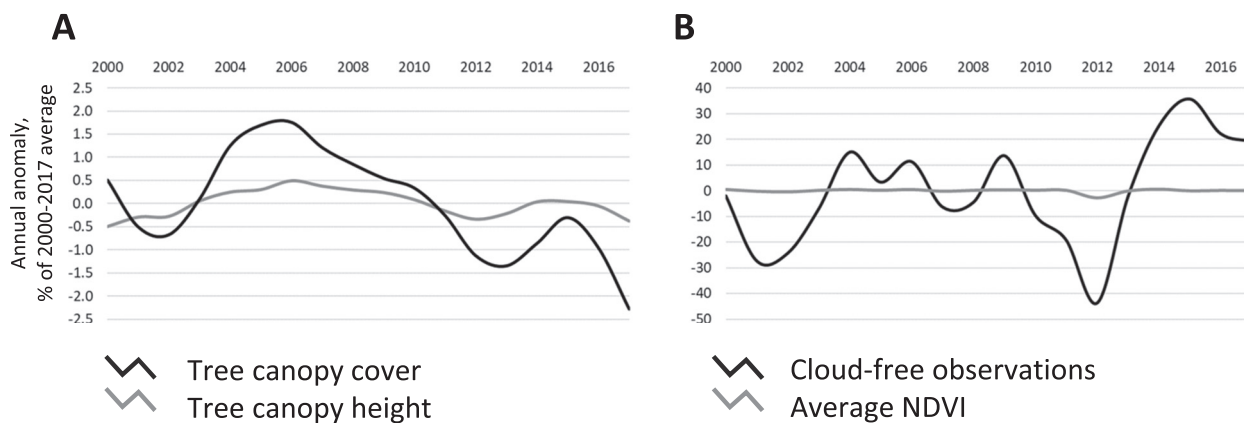
Fig. 12. A – Annual average tree canopy cover and tree canopy height within stable primary forests; percent difference from the 2000–2017 average. B – Number of clear-sky observations and average annual NDVI for all 3000 sample pixels used for the sample analysis; percent difference from the 2000–2017 average.

case, phenology-based reflectance metrics that are created using both pre- and post-disturbance observations may not provide sufficient information to map the effect of the change event to tree cover. Moreover, the timing of the event within the year and the availability of clear-sky observations before and after the disturbance event will affect change detection sensitivity. In the year following a disturbance event, rapid tree cover regeneration (especially, in case of forest plantations or shifting cultivation) can mask the signal of antecedent disturbance. Unlike annual tree canopy and height models, the annual change detection model is calibrated to detect abrupt losses of tree cover without respect to time of year. The change detection model in the current study was calibrated using training data that represented complete or near-complete canopy removal. Thus, we may use the model outputs as an indicator of a stand-level disturbance in a certain year. While our goal is to provide data users a tool to estimate forest area annually, we decided to assign tree cover and height values to zero for the years where such

stand-replacement disturbance were detected. The resulting dataset allows users to estimate net forest area change between any pair of years by direct inter-comparison of the annual tree cover and height maps.

4.4. Challenges of continuous vegetation structure monitoring

Temporal and spatial consistency allows data users to implement the presented data for (i) annual land cover and change mapping; (ii) national or regional stratification to support sample-based analysis; (iii) map calibration using regional lidar data, as available. A data user, however, should take into account the product limitations.

Some of the shortcomings of the calibration models were apparent during the mapping exercise. Since the model was calibrated with out-of-the-region training data, we may expect a bias in estimated tree cover and height. Our method assumes similarity of spectral response to
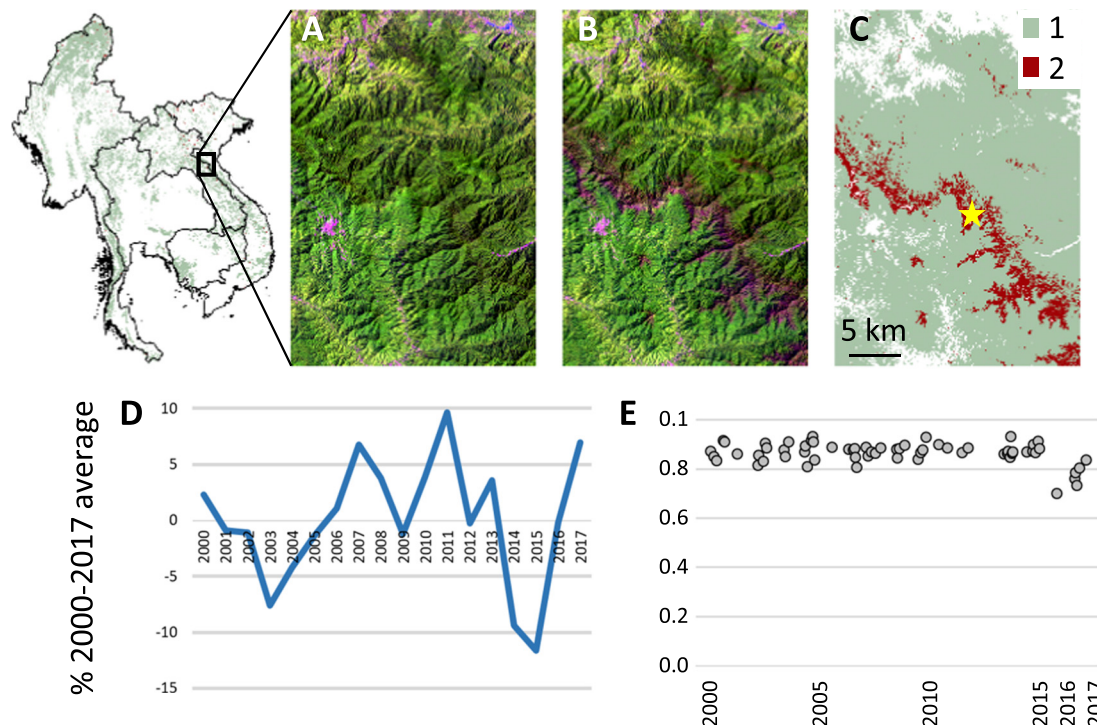

Fig. 13. Evidence of drought effect on the vegetation spectral reflectance. A-C Sample area in the Annamite Range on the border between Laos and Vietnam. A, B – Landsat image composites, 2015 and 2016; C – Primary forests extent (1) and primary forest areas where reduction of tree canopy cover by 5% or higher was observed in 2016/2017 compared to 2015 (2). D – Annual precipitation within Lower Mekong, percent of 2000–2017 average (data from Funk et al., 2015). E – NDVI for all 2000–2017 16-day clear-sky composites for a pixel marked with a start on the map C.

tree canopy structure between tropical forests. We suppose that if vegetation structure models were calibrated using within-region CHM data, the output maps may have had different values of canopy cover and height. The regional product that we derived using out-of-region calibration data should be considered a prototype. Regional lidar data, when it becomes available, may be used to re-calibrate the model following the presented approach.

Another source of model uncertainty is related to the aggregation of calibration high spatial resolution CHM data into Landsat 30 m spatial resolution. Calibration data for the tree cover model was derived as a proportion of a pixel covered with vegetation above 5 m height. The approach is similar to Matasci et al. (2018) who used a 2 m height threshold to map tree cover. As tree cover is defined using a strict threshold, the absolute error of the CHM model is critically important. The reported uncertainty of G-LiHT-derived digital terrain models is close to 3 m and even higher on slopes (Neigh et al., 2014). Thus, we may expect relatively high uncertainty of tree cover estimation for areas with average tree height at or near 5 m. We observed that the Landsat-scale canopy cover estimated from the CHM aggregation within dry and degraded forests of the Yucatan peninsula was low, even when high-resolution optical images (available on Google Earth) show dense canopy cover. The underestimation of canopy cover for the young, dry, or degraded forests with canopy heights close to 5 m may cause possible underestimation of canopy cover in young fallows within the Lower Mekong region.

Calibration of the tree cover height model is even more challenging. A number of variables can be extracted from the distribution of first return heights or CHM values within a Landsat pixel, including mean, median, maximum, etc. Some authors derived a set of models to predict different variables (Matasci et al., 2018). Our goal was to derive an annual time-series data that may be used at the national scale to map forests using specific structural definitions. We considered that a mean canopy height value would not be ideal for calibration as it mixes forested and non-forest areas. The maximum value would, in turn, lead to overestimation of forest area by highlighting pixels with just a few trees as forested. We decided to use 90% tree cover height value as a basis for model calibration. Overall, we conclude that there is no established single best method to derive canopy height calibration data at a 30 m resolution from the fine-resolution lidar data, and model calibration methods should be selected based on the expected application of the output map product.

5. Conclusion

We have presented an approach for annual Landsat-based woody vegetation structure monitoring for the Lower Mekong region (Cambodia, Laos, Myanmar, Thailand, and Vietnam) and prototyped it for the 2000–2017 time interval. The product was validated using regional-scale probability sampling which confirmed its suitability for national land cover monitoring applications. Our results confirm the importance of the long-term satellite data archive and phenological metrics for vegetation structure characterization and the value of tree cover loss detection for construction of consistent tree cover change time-series. The project results are available for download (https:// glad.umd.edu/) and serve as an input to the Lower Mekong Regional Land Cover Monitoring System (https://rlcms-servir.adpc.net/en/ forest-monitor/).

The primary obstacle in implementing the presented method to other regions of the world is the limited availability of lidar data. Here, we developed a model using lidar calibration data from outside of the region of study. Moving forward, vegetation structure data for the tropics and temperate biomes will be systematically collected by the Global Ecosystem Dynamics Investigation (GEDI) spaceborne lidar instrument (Qi et al., 2019). Improved multi-spectral data in terms of temporal and spatial resolution through the integration of Landsat and Sentinel-2 imagery is currently in development (Claverie et al., 2018).

Both the globally consistent lidar data for calibration and improved time-series optical data for estimation will enhance the mapping and monitoring capabilities presented here, with a global application feasible in the near term.

References

Breiman, L., 1996. Bagging predictors. Mach. Learn. 24, 123–140.

Breiman, L., Friedman, J.H., Olshen, R.A., Stone, C.J., 1984. Classification and Regression Trees. Wadsworth and Brooks/Cole, Monterey, California.

Brown, J.F., Loveland, T.R., Merchant, J.W., Reed, B.C., Ohlen, D.O., 1993. Using multisource data in global land-cover characterization - concepts, requirements, and methods. Photogramm. Eng. Remote Sens. 59, 977–987.

Carroll, M., Townshend, J.R.G., Hansen, M.C., DiMiceli, C., Sohlberg, R., Wurster, K., 2010. Vegetative cover conversion and vegetation continuous fields. In: Ramachandran, B., Justice, C., Abrams, M. (Eds.), Land Remote Sensing and Global Environmental Change: NASA's EOS and the Science of ASTER and MODIS. Springer, New York, pp. 725–745.

Chander, G., Markham, B.L., Helder, D.L., 2009. Summary of current radiometric calibration coefficients for Landsat MSS, TM, ETM+, and EO-1 ALI sensors. Remote Sens. Environ. 113 (5), 893–903.

Claverie, M., Ju, J., Masek, J.G., Dungan, J.L., Vermote, E.F., Roger, J.C., Skakun, S.V., Justice, C., 2018. The harmonized Landsat and Sentinel-2 surface reflectance data set. Remote Sens. Environ. 219, 145–161.

Cohen, W.B., Goward, S.N., 2004. Landsat's role in ecological applications of remote sensing. AIBS Bull. 54 (6), 535–545.

Cohen, W.B., Maiersperger, T.K., Gower, S.T., Turner, D.P., 2003. An improved strategy for regression of biophysical variables and Landsat ETM+ data. Remote Sens. Environ. 84, 561–571.

Colwell, R.N., 1993. Four decades of progress in photographic interpretation since the founding of commission VII (IP). Int. Arch. Photogramm. Remote. Sens. Spat. Inf. Sci. 29, 683.

Cook, B., Corp, L., Nelson, R., Middleton, E., Morton, D., McCorkel, J., Masek, J., Ranson, K., Ly, V., Montesano, P., Cook, B.D., Corp, L.A., Nelson, R.F., Middleton, E.M., Morton, D.C., McCorkel, J.T., Masek, J.G., Ranson, K.J., Ly, V., Montesano, P.M., 2013. NASA Goddard's LiDAR, hyperspectral and thermal (G-LiHT) airborne imager. Remote Sens. 5, 4045–4066.

Coulter, L.L., Stow, D.A., Tsai, Y.-H., Ibanez, N., Shih, H., Kerr, A., Benza, M., Weeks, J.R., Mensah, F., 2016. Classification and assessment of land cover and land use change in southern Ghana using dense stacks of Landsat 7 ETM+ imagery. Remote Sens. Environ. 184, 396–409.

DeFries, R.S., Townshend, J.R.G., 1994. NDVI-derived land cover classifications at a global scale. Int. J. Remote Sens. 15, 3567–3586.

DeFries, R., Hansen, M., Townshend, J., 1995. Global discrimination of land cover types from metrics derived from AVHRR pathfinder data. Remote Sens. Environ. 54, 209–222.

DeFries, R., Hansen, M., Townshend, J.R.G., Sohlberg, R., 1998. Global land cover classifications at 8 km spatial resolution: the use of training data derived from Landsat imagery in decision tree classifiers. Int. J. Remote Sens. 19 (16), 3141–3168.

DOF [Department of Forestry, Ministry of Agriculture and Forestry, Lao PDR], 2018. Lao PDR's forest reference emission level and forest reference level for REDD+ results payment under the UNFCCC. Available online: https://redd.unfccc.int/submissions. html.

FAO [Food and agriculture organization of the United Nations], 2001. Global Ecological Zoning for the Global Forest Resources Assessment 2000. UNFAO, Rome.

FAO [Food and agriculture organization of the United Nations], 2016. Global forest resources assessment 2015. UNFAO, Rome.

Foga, S., Scaramuzza, P.L., Guo, S., Zhu, Z., Dilley, R.D., Beckmann, T., Schmidt, G.L., Dwyer, J.L., Hughes, M.J., Laue, B., 2017. Cloud detection algorithm comparison and validation for operational Landsat data products. Remote Sens. Environ. 194, 379–390.

Friedl, M.A., McIver, D.K., Hodges, J.C., Zhang, X.Y., Muchoney, D., Strahler, A.H., Woodcock, C.E., Gopal, S., Schneider, A., Cooper, A., Baccini, A., 2002. Global land cover mapping from MODIS: algorithms and early results. Remote Sens. Environ. 83 (1–2), 287–302.

Funk, C., Peterson, P., Landsfeld, M., Pedreros, D., Verdin, J., Shukla, S., Husak, G., Rowland, J., Harrison, L., Hoell, A., Michaelsen, J., 2015. The climate hazards infrared precipitation with stations - a new environmental record for monitoring extremes. Scientific data 2, 150066.

GFOI [Global Forest Observations Initiative], 2016. Integration of Remote-Sensing and Ground-Based Observations for Estimation of Emissions and Removals of Greenhouse Gases in Forests: Methods and Guidance from the Global Forest Observations Initiative, Edition 2.0. Food and Agriculture Organization, Rome.

Giri, C., Ochieng, E., Tieszen, L.L., Zhu, Z., Singh, A., Loveland, T., Masek, J., Duke, N., 2011. Status and distribution of mangrove forests of the world using earth observation satellite data. Glob. Ecol. Biogeogr. 20 (1), 154–159.

Hansen, M.C., DeFries, R.S., Townshend, J.R.G., Marufu, L., Sohlberg, R., 2002a.

Development of a MODIS tree cover validation data set for Western Province, Zambia. Remote Sens. Environ. 83 (1–2), 320–335.

Hansen, M., DeFries, R., Townshend, J.R., Sohlberg, R., Dimiceli, C., Carroll, M., 2002b. Towards an operational MODIS continuous field of percent tree cover algorithm: examples using AVHRR and MODIS data. Remote Sens. Environ. 83, 303–319.

Hansen, M.C., DeFries, R.S., Townshend, J.R.G., Carroll, M., Dimiceli, C., Sohlberg, R.A., 2003. Global percent tree cover at a spatial resolution of 500 meters: first results of the MODIS vegetation continuous fields algorithm. Earth Interact. 7 (10), 1–15.

Hansen, M.C., Roy, D.P., Lindquist, E., Adusei, B., Justice, C.O., Altstatt, A., 2008. A method for integrating MODIS and Landsat data for systematic monitoring of forest cover and change in the Congo Basin. Remote Sens. Environ. 112 (5), 2495–2513.

Hansen, M., Stehman, S., Potapov, P., 2010. Quantification of global gross forest cover loss. Proc. Natl. Acad. Sci. U. S. A. 107 (19), 8650–8655.

Hansen, M., Potapov, P.V., Moore, R., Hancher, M., Turubanova, S.A.A., Tyukavina, A., Thau, D., Stehman, S.V., Goetz, S.J., Loveland, T.R., Kommareddy, A., 2013. High-resolution global maps of 21st-century forest cover change. Science 342 (6160), 850–853.

Hansen, M.C., Potapov, P.V., Goetz, S.J., Turubanova, S., Tyukavina, A., Krylov, A., Kommareddy, A., Egorov, A., 2016. Mapping tree height distributions in Sub-Saharan Africa using Landsat 7 and 8 data. Remote Sens. Environ. 185, 221–232.

Huang, C., Goward, S.N., Masek, J.G., Thomas, N., Zhu, Z., Vogelmann, J.E., 2010. An automated approach for reconstructing recent forest disturbance history using dense Landsat time series stacks. Remote Sens. Environ. 114, 183–198.

Hudak, A.T., Lefsky, M.A., Cohen, W.B., Berterretche, M., 2002. Integration of lidar and Landsat ETM+ data for estimating and mapping forest canopy height. Remote Sens. Environ. 82, 397–416.

Huete, A., Justice, C.O., Van Leeuwen, W., 1999. Modis Vegetation Index (Mod 13) Algorithm Theoretical Basis Document. University of Arizona/University of Virginia.

IPCC [Intergovernmental Panel on Climate Change], 2006. In: Eggleston, H.S., Buendia, L., Miwa, K., Ngara, T., Tanabe, K. (Eds.), IPCC Guidelines for National Greenhouse gas Inventories. Institute for Global Environmental Strategies, Hayama.

Iverson, L.R., Graham, R.L., Cook, E.A., 1989. Applications of satellite remote sensing to forested ecosystems. Landsc. Ecol. 3 (2), 131–143.

Justice, C.O., Townshend, J.R.G., Holben, B.N., Tucker, C.J., 1985. Analysis of the phenology of global vegetation using meteorological satellite data. Int. J. Remote Sens. 6, 1271–1318.

Justice, C.O., Townshend, J.R.G., Vermote, E.F., Masuoka, E., Wolfe, R.E., Saleous, N., Roy, D.P., Morisette, J.T., 2002. An overview of MODIS land data processing and product status. Remote Sens. Environ. 83 (1–2), 3–15.

Kennedy, R.E., Yang, Z., Cohen, W.B., 2010. Detecting trends in forest disturbance and recovery using yearly Landsat time series: 1. LandTrendr - temporal segmentation algorithms. Remote Sens. Environ. 114, 2897–2910.

Loveland, T.R., Belward, A.S., 1997. The IGBP-DIS global 1km land cover data set, DISCover: first results. Int. J. Remote Sens. 18, 3289–3295.

MARD [Ministry of Agriculture and Rural Development of Vietnam], 2016. Vietnam's modified submission on reference levels for REDD+ results-based payments under UNFCCC. Available online: https://redd.unfccc.int/submissions.html.

Masek, J.G., Vermote, E.F., Saleous, N.E., Wolfe, R., Hall, F.G., Huemmrich, K.F., Gao, F., Kutler, J., Lim, T.-K., 2006. A Landsat surface reflectance dataset for North America, 1990–2000. IEEE Geosci. Remote Sens. Lett. 3, 68–72.

Matasci, G., Hermosilla, T., Wulder, M.A., White, J.C., Coops, N.C., Hobart, G.W., Zald, H.S.J., 2018. Large-area mapping of Canadian boreal forest cover, height, biomass and other structural attributes using Landsat composites and lidar plots. Remote Sens. Environ. 209, 90–106.

MOE [Ministry of Environment, Cambodia], 2017. Initial forest reference level for Cambodia under the UNFCCC framework. Available online: https://redd.unfccc.int/submissions.html.

MONREC [Ministry of Natural Resources and Environmental Conservation of Myanmar], 2018. Forest Reference Emission Level (FREL) of Myanmar. Available online: https://redd.unfccc.int/submissions.html.

Neigh, C., Masek, J., Bourget, P., Cook, B., Huang, C., Rishmawi, K., Zhao, F., Neigh, C.S.R., Masek, J.G., Bourget, P., Cook, B., Huang, C., Rishmawi, K., Zhao, F., 2014. Deciphering the precision of stereo IKONOS canopy height models for US forests with G-LiHT airborne LiDAR. Remote Sens. 6, 1762–1782.

Olofsson, P., Foody, G.M., Herold, M., Stehman, S.V., Woodcock, C.E., Wulder, M.A., 2014. Good practices for estimating area and assessing accuracy of land change. Remote Sens. Environ. 148, 42–57.

Pickering, J., Stehman, S.V., Tyukavina, A., Potapov, P., Watt, P., Jantz, S.M., Bholanath, P., Hansen, M.C., 2019. Quantifying the trade-off between cost and precision in estimating area of forest loss and degradation using probability sampling in Guyana. Remote Sens. Environ. 221, 122–135.

Potapov, P.V., Turubanova, S.A., Hansen, M.C., Adusei, B., Broich, M., Altstatt, A., Mane, L., Justice, C.O., 2012. Quantifying forest cover loss in Democratic Republic of the Congo, 2000–2010, with Landsat ETM+ data. Remote Sens. Environ. 122, 106–116.

Potapov, P.V., Dempewolf, J., Talero, Y., Hansen, M.C., Stehman, S.V., Vargas, C., Rojas, E.J., Castillo, D., Mendoza, E., Calderón, A., Giudice, R., Malaga, N., Zutta, B.R., 2014. National satellite-based humid tropical forest change assessment in Peru in support of REDD+ implementation. Environ. Res. Lett. 9.

Potapov, P.V., Turubanova, S.A., Tyukavina, A., Krylov, A.M., McCarty, J.L., Radeloff, V.C., Hansen, M.C., 2015. Eastern Europe's forest cover dynamics from 1985 to 2012 quantified from the full Landsat archive. Remote Sens. Environ. 159, 28–43.

Potapov, P., Siddiqui, B.N., Iqbal, Z., Aziz, T., Zzaman, B., Islam, A., Pickens, A., Talero, Y., Tyukavina, A., Turubanova, S., Hansen, M.C., 2017. Comprehensive monitoring of Bangladesh tree cover inside and outside of forests, 2000-2014. Environ. Res. Lett. 12, 2000–2014.

Qi, W., Lee, S.K., Hancock, S., Luthcke, S., Tang, H., Armston, J., Dubayah, R., 2019. Improved forest height estimation by fusion of simulated GEDI Lidar data and TanDEM-X InSAR data. Remote Sens. Environ. 221, 621–634.

Reese, H., Nilsson, M., Pahlén, T.G., Hagner, O., Joyce, S., Tingelöf, U., Egberth, M., Olsson, H., 2003. Countrywide estimates of forest variables using satellite data and field data from the national forest inventory. AMBIO 32, 542–548.

Running, S.W., Nemani, R.R., Heinsch, F.A., Zhao, M., Reeves, M., Hashimoto, H., 2004. A continuous satellite-derived measure of global terrestrial primary production. AIBS Bull. 54 (6), 547–560.

SERVIR-Mekong, 2015. A Needs Assessment of Geospatial Data and Technologies in the Lower Mekong Region. ADPC, Bangkok.

Simard, M., Pinto, N., Fisher, J.B., Baccini, A., 2011. Mapping forest canopy height globally with spaceborne lidar. J. Geophys. Res. 116, 4021.

Skole, D., Tucker, C., 1993. Tropical deforestation and habitat fragmentation in the Amazon: satellite data from 1978 to 1988. Science 260, 1905–1910.

Souza Jr., C.M., Roberts, D.A., Cochrane, M.A., 2005. Combining spectral and spatial information to map canopy damage from selective logging and forest fires. Remote Sens. Environ. 98 (2–3), 329–343.

Stehman, C.V., 2014. Estimating area and map accuracy for stratified random sampling when the strata are different from the map classes. Int. J. Remote Sens. 35, 4923–4939.

Thirumalai, K., DiNezio, P.N., Okumura, Y., Deser, C., 2017. Extreme temperatures in Southeast Asia caused by El Nino and worsened by global warming. Nat. Commun. 8, 15531.

Tomppo, E., Olsson, H., Ståhl, G., Nilsson, M., Hagner, O., Katila, M., 2008. Combining national forest inventory field plots and remote sensing data for forest databases. Remote Sens. Environ. 112, 1982–1999.

Tucker, C.J., Holben, B.N., Goff, T.E., 1984. Intensive forest clearing in Rondonia, Brazil, as detected by satellite remote sensing. Remote Sens. Environ. 15, 255–261.

Turubanova, S., Potapov, P.V., Tyukavina, A., Hansen, M.C., 2018. Ongoing primary forest loss in Brazil, Democratic Republic of the Congo, and Indonesia. Environ. Res. Lett. 13, 074028.

Tyukavina, A., Stehman, S.V., Potapov, P.V., Turubanova, S.A., Baccini, A., Goetz, S.J., Laporte, N.T., Houghton, R.A., Hansen, M.C., 2013. National-scale estimation of gross forest above ground carbon loss: a case study of the Democratic Republic of the Congo. Environ. Res. Lett. 8, 044039.

Verbesselt, J., Hyndman, R., Newnham, G., Culvenor, D., 2010. Detecting trend and seasonal changes in satellite image time series. Remote Sens. Environ. 114, 106–115.

Westman, W.E., Strong, L.L., Wilcox, B.A., 1989. Tropical deforestation and species endangerment: the role of remote sensing. Landsc. Ecol. 3, 97–109.

Woodcock, C.E., Allen, R., Anderson, M., Belward, A., Bindschadler, R., Cohen, W., Gao, F., Goward, S.N., Helder, D., Helmer, E., Nemani, R., Oreopoulos, L., Schott, J., Thenkabail, P.S., Vermote, E.F., Vogelmann, J., Wulder, M.A., Wynne, R., 2008. Free access to Landsat imagery. Science 320, 1011.

Wulder, M.A., Han, T., White, J.C., Sweda, T., Tsuzuki, H., 2007. Integrating profiling LIDAR with Landsat data for regional boreal forest canopy attribute estimation and change characterization. Remote Sens. Environ. 110, 123–137.

Wulder, M.A., Masek, J.G., Cohen, W.B., Loveland, T.R., Woodcock, C.E., 2012. Opening the archive: how free data has enabled the science and monitoring promise of Landsat. Remote Sens. Environ. 122, 2–10.

Wulder, M.A., Coops, N.C., Roy, D.P., White, J.C., Hermosilla, T., 2018. Land cover 2.0. Int. J. Remote Sens. 39, 4254–4284.

Xu, L., Saatchi, S.S., Shapiro, A., Meyer, V., Ferraz, A., Yang, Y., Bastin, J.-F., Banks, N., Boeckx, P., Verbeeck, H., Lewis, S.L., Muanza, E.T., Bongwele, E., Kayembe, F., Mbenza, D., Kalau, L., Mukendi, F., Ilunga, F., Ebuta, D., 2017. Spatial distribution of carbon stored in forests of the Democratic Republic of Congo. Sci. Rep. 7, 15030.